

Population transfer in a level-crossing model with two time scales

K.-A. Suominen and B. M. Garraway

Research Institute for Theoretical Physics, University of Helsinki, Siltavuorenpenger 20 C, SF-00170 Helsinki, Finland

(Received 17 May 1991)

We set up a level-crossing model with two time scales and compare the numerically calculated probability transfer with several analytic results. We also examine the probability transfer in the adiabatic limit and make a comparison with a calculation based on the approach of Dykhne [Sov. Phys.—JETP **11**, 411 (1960); **14**, 941 (1962)] and of Davis and Pechukas [J. Chem. Phys. **64**, 3129 (1976)]. We find that we can get an improved agreement if we modify their approach.

PACS number(s): 32.80.Bx, 33.80.Be, 42.50.—p

I. INTRODUCTION

The behavior of simple quantum systems in the adiabatic limit has become of some interest recently. This is particularly so because of the awareness of the geometric phase in quantum mechanics [1]. We have been interested in extending our understanding of the general behavior of two-level systems in the adiabatic limit, and in seeing which universal features they share. This has resulted in the study of an increasing number of models, including those found in Refs. [2,3]. In this paper we present a generalized pulse model with two separate time scales and we see how it relates to other known models, how it behaves in the adiabatic limit, and how its general behavior may be understood.

We may envisage a number of different physical situations. For example, we could have an experiment where an atom (or molecule) interacts with a laser pulse. Provided the pulse is not too short, the atomic system may be simplified to a two-level problem with a coupling between the levels that is dependent on the electric-field amplitude of the light pulse. If we change the frequency of the light pulse, we will effectively induce a time dependence into the energies of the two levels that would cause them to cross if the laser sweeps through resonance (see, for example, Refs. [4,5]). Another example of a physical system can be found in the crossing of Rydberg energy levels caused by the application of an external field [6,7]. By manipulating this field, we can control the way the system passes through a level crossing.

The prototype of all level-crossing problems is the Landau-Zener system [8]. In this model one assumes a constant coupling and energy levels that cross linearly in time. This means that the model contains several absurdities; it is unrealistic to have infinite energies as $t \rightarrow \pm \infty$, or a constant coupling that never turns off. However, the problem is analytically solvable and yields sensible answers. From a physical point of view it does this because only the behavior of the system near the crossing is important when considering the final transfer of probability between the levels. This allows physical applications of the model because, over a small enough time scale, al-

most any crossing system will have a linear dependence in its energy levels and a constant interaction. However, the Landau-Zener model cannot be correct if the time scale over which the processes important to probability transfer occur is greater than the linear region of the model. Further, the Landau-Zener problem gives no clue as to how applicable it may be in practice.

It is with this in mind that we consider a model with a linear region near the crossing, but with finite energies at large times. This is similar to the system studied in Ref. [6], except that we have a pulsed coupling that acts over a finite time scale. This time scale is not connected to the time scale over which the crossing is linear—unlike the pulsed model we studied in Ref. [3].

In the following section we shall discuss the general behavior of the two-time-scale model. In particular we shall see how it can relate to the Landau-Zener model, what its behavior is like in various limits, and how it relates to other models with analytic solutions. Then in the third section we will discuss concepts of adiabaticity and we will show how the model approaches the adiabatic limit. A comparison of the exact numerical behavior will be made with nonperturbative predictions. Finally, Sec. IV contains some concluding remarks.

II. THE TWO-TIME-SCALE MODEL, RELATED MODELS, AND THEIR BEHAVIOR

First we shall set up the formalism and notation for the problem. The whole class of two-level problems without dissipation can be described by the Hamiltonian

$$H(t) = \begin{pmatrix} \alpha(t) & V(t) \\ V(t) & -\alpha(t) \end{pmatrix}. \quad (1)$$

The symmetric form of Eq. (1) can always be achieved with the aid of suitable transformations. The state vector

$$\Psi(t) = \begin{pmatrix} C_1(t) \\ C_2(t) \end{pmatrix} \quad (2)$$

will satisfy the Schrödinger equation of motion (with $\hbar=1$)

$$i \frac{d\Psi(t)}{dt} = H(t)\Psi(t) . \tag{3}$$

This equation of motion is not trivially solved when α or V are functions of time. Apart from some special exceptions, we must solve the two coupled first-order linear differential equations in Eq. (3) by numerical methods such as Runge-Kutta integration. However, in this paper we will also describe nontrivial analytic solutions of a few of the special cases, in order to show their relevance to the more general model.

We choose as initial conditions

$$C_1(-\infty)=1, \quad C_2(-\infty)=0 , \tag{4}$$

and the time-dependent probabilities will be $P_1(t)=|C_1(t)|^2$ and $P_2(t)=|C_2(t)|^2$. We shall also define

$$P = P_1(\infty) \tag{5}$$

as the probability of the system remaining in level 1 after the whole crossing process is over. As we have a single crossing of the levels, the quantity P will be very small as we approach the adiabatic limit, corresponding to a vanishing transfer of population in the adiabatic basis.

The function $\alpha(t)$ in Eq. (1) is interpreted as the energy of one of the two levels in the simplified atomic system, and the function $V(t)$ is a time-dependent coupling between the levels. The particular form of these functions for the two-time-scale model treated in this paper will be

$$\begin{aligned} \alpha &= E_0 \tanh(t/T_1) , \\ V &= V_0 \operatorname{sech}(t/T_2) , \end{aligned} \tag{6}$$

as is illustrated in Fig. 1(a). We see that the two levels 1 and 2 start at $t = -\infty$ with finite energies $\pm E_0$. Near $t=0$ there is a crossing of the energy levels that takes place over a time scale T_1 . There is no coupling except during a time of the order T_2 around $t=0$. The param-

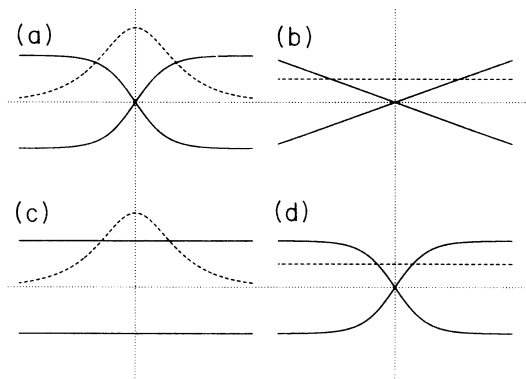


FIG. 1. This figure illustrates the different types of models that we discuss in this paper. The function $\alpha(t)$ is shown in the solid curves, and $V(t)$ is shown in the dashed curves. The models are (a) the two-time-scale model, or, with equal time-scales, the first Demkov-Kunike (or DK1) model; (b) the Landau-Zener model; (c) the Rosen-Zener model; (d) the second Demkov-Kunike (or DK2) model.

eter T_2 gives the second time scale. At $t=0$ the coupling is at its maximum and has the value V_0 .

We note that the two-time-scale problem, as defined by Eqs. (6), has four parameters, of which only three are significant. This is because we are only interested in the final transition probability and so by scaling time we can eliminate one of the free parameters. If we choose the scaling so that $t \rightarrow \beta t$ we will find that the final transition probability is unchanged if the parameters are scaled as

$$\begin{aligned} E_0 &\rightarrow E_0/\beta , \\ V_0 &\rightarrow V_0/\beta , \\ T_1 &\rightarrow \beta T_1 , \\ T_2 &\rightarrow \beta T_2 . \end{aligned} \tag{7}$$

In our numerical work we have chosen $\beta = E_0$ so that E_0 is effectively fixed at a value of unity. We note that combinations of parameters such as $V_0 T_2, E_0 T_1, E_0 T_2$, and $V_0^2 T_1 / E_0$ are invariant under the scaling.

One of the special cases of Eq. (1) with an analytic solution is the Landau-Zener model which may be defined by [see Fig. 1(b)]

$$\begin{aligned} \alpha &= \lambda t , \\ V &= V_0 . \end{aligned} \tag{8}$$

Here the parameter λ gives the slope of the crossing, and the coupling V shows no time dependence. The solution to the differential equations is in terms of parabolic cylinder functions and it may be shown that the probability of remaining in level 1 is [8]

$$P = \exp(-\pi\Lambda) , \tag{9}$$

where we have defined an ‘‘adiabaticity’’ parameter

$$\Lambda = V_0^2 / \lambda . \tag{10}$$

Note that as the adiabaticity parameter Λ increases, the population in level 1 decreases. A high degree of adiabaticity may be achieved in *two* ways: the coupling V_0 may be very large, or, as expected intuitively, the rate of change of the energy levels λ may be very small.

In our previous work [2,3] we have noted that there is a time scale associated with the Landau-Zener model that is of the order of V_0/λ . This is the time, measured from the crossing, when the energies of the two levels and the coupling energy are equal in magnitude, and it appears to be the time scale over which nonadiabatic processes take place. As a result, we may suppose that the two-time-scale model defined in Eq. (6) will produce a probability transfer close to the prediction from the Landau-Zener model when this time scale is somewhat shorter than the times T_1 and T_2 . Thus to make a comparison between the two-time-scale model and the Landau-Zener model we should set $\lambda = E_0/T_1$ so that $\Lambda = V_0^2 T_1 / E_0$ is the Landau-Zener adiabaticity parameter. Then the final population of level 1 is determined by Eq. (9) provided that

$$V_0 T_1 / E_0 \ll (T_1, T_2) . \tag{11}$$

However, it turns out that this condition is not sufficient.

We can check the validity of the argument above by considering a special case of the two-time-scale model where $T_1 = T_2$, and the single time scale is given the label T . This model, defined by

$$\begin{aligned}\alpha &= E_0 \tanh(t/T), \\ V &= V_0 \operatorname{sech}(t/T),\end{aligned}\quad (12)$$

was discussed in Ref. [3], and it is one of the few examples having an analytic solution. To our knowledge, the first people to derive the result were Demkov and Kunike in 1969 [9], (followed more recently by Hioe and Carrol [10]), and so we shall refer to this model as the DK1 model. Because their paper is not, we believe, widely available, we have reproduced some of the details of their solution in Appendix A in this paper. Presently, we only require the result for the probability of nontransfer which is [Eq. (A11) with $a=0, b=E_0, c=V_0$]

$$P = \frac{\cosh^2 \pi T (E_0^2 - V_0^2)^{1/2}}{\cosh^2 \pi T E_0}. \quad (13)$$

As a function of increasing V_0 , this probability at first falls from unity until $V_0 > E_0$, when characteristic oscillations are seen with a constant amplitude of $\operatorname{sech}^2 \pi T E_0$. In Ref. [3] we showed how each of these oscillations was connected to an integer number of precessions of the Bloch vector during the time evolution.

We now examine the limit $V_0/E_0 \ll 1$ in Eq. (11) and expand the square root in Eq. (13) in powers of V_0/E_0 , so that to a first approximation

$$P \rightarrow \left[\cosh \frac{\pi}{2} \Lambda - \sinh \frac{\pi}{2} \Lambda \tanh \pi T E_0 \right]^2, \quad (14)$$

where $\Lambda = V_0^2 T / E_0$ is the adiabaticity constant anticipated from a linearization. We will only obtain the Landau-Zener result if we have the additional constraint

$$\pi T E_0 \gg 1, \quad (15)$$

so that the hyperbolic tangent becomes close to unity. This constraint will be broken if either the linear region is too narrow or the energy separation of the two levels is too small. As we have already taken the size of the crossing into account, it seems that a small time scale T must be having some other effect.

The resolution of this problem lies in the fact that short pulses tend to generate nonadiabatic transitions. Thus if the rise of the secant pulse is too sudden, the Landau-Zener result is not obtained because of nonadiabatic transfer prior to reaching the crossing region. This transfer ensures that when we do reach the crossing region, the initial conditions for the Landau-Zener model have not effectively been met; in the Landau-Zener model we expect to have adiabatic following until we reach the crossing region. If another model is going to converge on the Landau-Zener limit, it should approach the crossing region in an adiabatic manner, as happens in the Landau-Zener model.

We can gain some qualitative insight into this by con-

sidering yet another analytically solvable model, the Rosen-Zener model [11]. The model is defined by having atomic energies that are constant while the coupling follows a secant pulse as shown in Fig. 1(c). Thus we have

$$\begin{aligned}\alpha &= E_0 \\ V &= V_0 \operatorname{sech}(t/T_2).\end{aligned}\quad (16)$$

In this case there is *no* crossing and the transfer of probability from one level to the other is caused entirely by nonadiabatic effects from the coupling. Because of this, there is no Landau-Zener limit to this model. The exact solution shows that the final probability of remaining in the level 1 is given by

$$P = 1 - \frac{\sin^2 \pi T_2 V}{\cosh^2 \pi T_2 E_0}. \quad (17)$$

To show that adiabatic following takes place up to the crossing, we should be interested in the nonadiabatic transfer near $t=0$, so that only the rising part of the secant is considered. However, the probability at $t=\infty$ does give a qualitative result, even though it contains the effects of both the rising and falling parts of the pulsed coupling. We can see that a condition like Eq. (15) is sufficient to ensure that the Rosen-Zener probability P in Eq. (17) is close to unity. [We do not concern ourselves with the other possibility in Eq. (16), namely that $\sin^2 \pi T_2 V \ll 1$. Such a condition would either mean that the coupling was very small or that the precessions of the Bloch vector, having been caused by nonadiabatic effects, just happen to result in no transfer. This is the case with $2\pi, 4\pi, 6\pi$, etc. pulses, which are not adiabatic.]

So far as the two-time-scale model is concerned, we may conclude that we expect to find the Landau-Zener result as long as conditions (11) and (15) are satisfied. From the Rosen-Zener model we may see that the time scale in Eq. (15) should include T_2 . Whether Eq. (15) also needs to be satisfied with T replaced by T_1 is a question that remains to be answered.

In order to see what happens in practice, we show in Fig. 2 how the probability transfer in the two-time-scale model can be approximated by results from two other models and for four different values of $T_1 E_0$. The region delineated by the solid line belongs to the second Demkov-Kunike model, which we shall discuss further shortly. The region that is closely approximated by the Landau-Zener model is shown above the dotted line. We have determined this region by evaluating the fraction $\Delta P/P$, where P is the numerically calculated probability from the two-time-scale model, and ΔP is the difference between P and the Landau-Zener prediction Eq. (9). The dotted boundary marks where the relative error is small and $\Delta P/P = 10^{-3}$. We note that as $V_0 \rightarrow 0$, both the numerical P and the Landau-Zener prediction approach the same value of unity. This means there is a perfect agreement in that limit, and there may be other accidental agreements such as the one leading to the sharp spikes seen in Fig. 2 when $T_1 E_0 = 0.01$.

The Landau-Zener region extends over a wide range of T_2 but within small values of V_0 . For small values of T_2

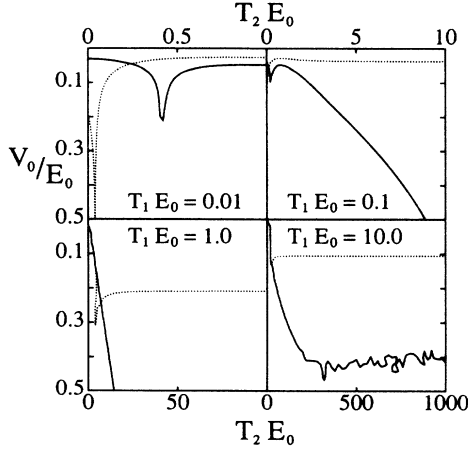


FIG. 2. This figure shows regions over which the Landau-Zener model and the DK2 model [defined in Eq. (18)] may be used to approximate the final probability in the two-time-scale model. The four parts of the figure show four different values of $T_1 E_0$. In each case, the DK2 model gives a good approximation to the final probability above the solid line, and the Landau-Zener model gives a good approximation above the dotted line. The lines show where $\Delta P/P = 10^{-3}$; P is the probability in level 1, and ΔP is the difference between this probability and that found from the model being compared.

the second part of the bound (11) involving T_2 restricts the Landau-Zener region to a steep boundary. As T_2 increases, the boundary is affected by the first part of Eq. (11), which constrains V_0 to small values. Condition (15) with T_1 is the reason for the smallness of the Landau-Zener region when $T_1 E_0 = 0.01$ and $T_1 E_0 = 0.1$.

The region marked by the solid curve on Fig. 2 belongs to the second model for which Demkov and Kunike also found an analytic solution [9]; we shall call it the DK2 model. The figure shows that the DK2 model generally provides a better description of the final probability than the Landau-Zener model. It retains the time dependence on the diagonal part of the two-time-scale Hamiltonian, rather than on the off-diagonal part, and is defined by

$$\begin{aligned} \alpha &= E_0 \tanh(t/T_1), \\ V &= V_0, \end{aligned} \quad (18)$$

as illustrated in Fig. 1(d). This model is not a limit of the two-time-scale model. While Eqs. (6) do formally go over into Eqs. (18) in the limit $T_2 \rightarrow \infty$, the two models can never have comparable initial conditions. This is because the DK2 model always starts with a finite coupling at $t = -\infty$ and in an initial adiabatic state, whereas the two-time-scale model starts with zero coupling. The treatment of Demkov and Kunike [9] gives the final transition probability in the adiabatic basis as [Eq. (A17) with $a = 0, b = E_0, c = V_0$]

$$P = \frac{\sinh^2 \pi T_1 E_0}{\sinh^2 [\pi T_1 (E_0^2 + V_0^2)^{1/2}]} \quad (19)$$

Unlike the DK1 and Rosen-Zener models, the final prob-

ability P shows *no* oscillations as a function of its parameters. The two-time-scale model can go over into the DK2 model if there is an adiabatic following of the secant pulse and if the pulse is broad compared to the time scale of the hyperbolic crossing in the two-time-scale model. For the former condition we have the same constraint on T_2 as we found in the Rosen-Zener model. That the pulse be broad simply requires

$$T_2 \gg T_1. \quad (20)$$

This latter condition is satisfied over most of the regions shown in Fig. 2. The former condition, $\pi T_2 E_0 \gg 1$, is also mostly satisfied in Fig. 2. However, the DK2 region shown for $T_1 E_0 = 0.01$ hardly satisfies this condition and is thus reduced to a small area where the agreement appears accidental. The peaks seen in the DK2 boundary for $T_1 E_0 = 0.01$ and $T_1 E_0 = 0.1$ are coincidences caused by a crossing of the DK2 result with the result from the two-time-scale model. The same relative criterion $\Delta P/P = 10^{-3}$, was used to determine the DK2 boundary as was used for the boundary of the Landau-Zener region. The irregular behavior seen when $T_1 E_0 = 10.0$ occurs because P itself has become quite small (around $10^{-4} - 10^{-6}$) and the comparison becomes difficult.

That the two-time-scale model can mimic the DK2 model is illustrated in Fig. 3 where we can see the probability in level 1 as a function of time. Three cases are shown where there is nearly complete transfer of probability. In Fig. 3(a) condition (20) is satisfied and the two time scales are well separated. For $t E_0 \lesssim 0$ the probability changes smoothly and slowly because of the adiabatic following. The behavior reflects the secant time dependence of the pulse shape. However, as the system approaches the crossing there is some nonadiabatic transfer

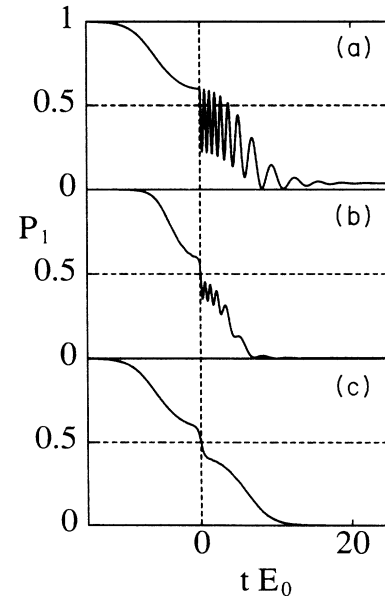


FIG. 3. The time development of P_1 when $V_0/E_0 = 5.0$ and (a) $T_1 E_0 = 0.01, T_2 E_0 = 3.0$; (b) $T_1 E_0 = 0.2, T_2 E_0 = 2.0$; (c) $T_1 E_0 = 0.5, T_2 E_0 = 3.0$. The final probability is near to that given by the DK2 model in each case.

resulting in the oscillations and the finite value of P_1 at the end. The oscillations die out as the coupling between the levels disappears. For this reason the diabatic and adiabatic states become the same and the DK2 result Eq. (19) (given in the adiabatic basis) applies. It accurately predicts a value of $P=0.038$ in Fig. 3(a). In Figs. 3(b) and 3(c) we have increased the value of T_1 ; this results in a smoother time dependence of the energy and in increasingly adiabatic transfer. Thus the amplitude of the oscillations decreases as we increase T_1 . However, in Fig. 3(b) we have slightly reduced T_2 , so that the condition $\pi T_2 E_0 \gg 1$ is encroached upon. The secant pulse now rises sufficiently rapidly to cause some nonadiabatic transitions prior to reaching the crossing, which results in the very small ripples seen for $tE_0 \lesssim 0$. This means that the initial condition for the DK2 model, i.e., an adiabatic eigenstate, is no longer met and the transfer is not quite given by the DK2 formula.

We can find Landau-Zener behavior as a limit of the DK2 model. If the constraints (11) are applied to the DK2 result Eq. (19), P reduces to the Landau-Zener transition probability, as it did in the DK1 case. This is why the DK2 region in Fig. 2 generally encompasses the Landau-Zener region. It extends further outwards to large V_0 because the model still applies even if Eq. (11) is violated, provided that Eq. (15) (with $T \rightarrow T_2$) and Eq. (20) are not. This is because the crossing region in the DK2 model may be larger than the time scale T_1 . As a

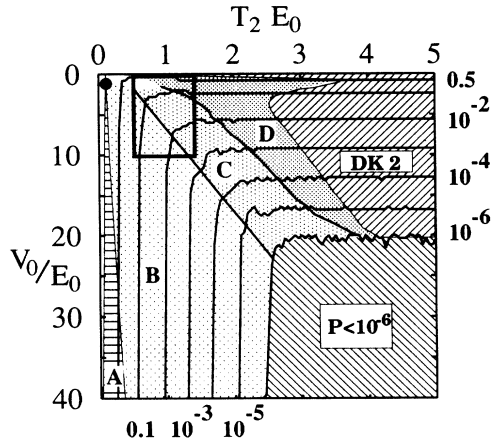


FIG. 4. This diagram shows how the final probability may be characterized over a region of the parameter space with $T_1 E_0 = 0.1$. The axes for V_0/E_0 and $T_2 E_0$ are to the left-hand side and above, respectively. The numbers displayed on the right-hand side and below are values belonging to the contour lines. The contours themselves are found by taking peak values when oscillatory behavior is present (in regions A, B, C, and D). The computational precision prevents any designation to the region in the bottom right-hand-side corner. The rectangle near the top left-hand-side corner shows the area covered by Fig. 6. The black dot marks the exceptional point discussed in the text. Regions A and B exhibit behavior related to the DK1 model. Regions C and D show complex oscillatory structures that do not belong to any simple model, but that may be partially described using the methods of Sec. III.

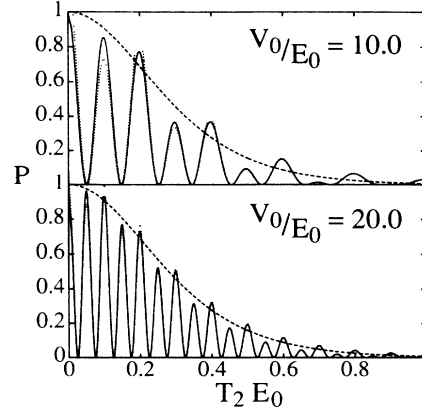


FIG. 5. This figure shows the final probability for the quite small value of $T_1 E_0 = 0.01$ and two large values of V_0/E_0 . The oscillating solid line shows the numerical result from the two-time-scale model, and the dashed curve that nearly matches the envelope of the oscillations is the envelope found in the DK1 model [i.e., the secant part of Eq. (21)]. The closely fitting dotted curve comes from the modified DDP treatment, and is discussed in Sec. III.

result, we may say that the DK2 model has a wider applicability than the Landau-Zener model.

In Fig. 4 we show the different types of behavior of the two-time-scale model as a function of the parameters $T_2 E_0$ and V_0/E_0 . The parameter $T_1 E_0$ has been fixed at the nontrivial value of 0.1; for higher values of $T_1 E_0$ we find that the interesting effects are lost. The DK2 region is shown over a wider range of V_0/E_0 than in the corresponding part of Fig. 2, allowing us to include other features of the model. We have omitted the Landau-Zener region from the diagram because it is quite small and lies within the DK2 region. The region marked $P < 10^{-6}$ indicates where the final probability was so small that we could not make a reliable comparison between the numerical result and the analytic formulas. However, the trends from the other parts of the diagram are clear.

The vertical wedge A shows the region where the DK1 model is found to be applicable for a tolerance $\Delta P/P = 0.01$. This region naturally surrounds the line given by $T_2 = T_1$ where the DK1 model is a special case of the two-time-scale model. The DK1 model is still applicable because differences in time scales have no appreciable effect there. As we noted in Ref. [3], the DK1 model has an exceptional point when $E_0 = V_0$, where if we transfer to an adiabatic basis we will find the Rosen-Zener equations. This special point is marked with a black dot in Fig. 4. We will discuss the adiabatic basis further in the following section.

In the region marked B we find oscillations in the final probability both as a function of $T_2 E_0$ and V_0/E_0 . The amplitude of the oscillations, which has been approximated by the contour lines, has an almost exponential falloff as a function of $T_2 E_0$. This behavior is well described by an application of the DK1 formula Eq. (13),

$$P = \frac{\cosh^2 \pi T_2 (E_0^2 - V_0^2)^{1/2}}{\cosh^2 \pi T_2 E_0}, \quad (21)$$

which includes the oscillations as a function of V_0/E_0 and $T_2 E_0$, and their amplitude as a function of $T_2 E_0$. The applicability of this equation at low $T_1 E_0$ is shown in Fig. 5 where Eq. (21) gives the secant fit to the envelope of the oscillations as a function of $T_2 E_0$. The fit is not so good as V_0/E_0 decreases, which corresponds to moving towards the region C in Fig. 4.

Close to the boundary of regions B and C half the oscillations disappear as may be seen in Fig. 6. This figure shows the probability P as a surface plot in a portion of the $(T_2 E_0, V_0/E_0)$ parameter space represented by the rectangle on Fig. 4. Because of the suppression of half of the oscillations the ripples in Fig. 6 show alternating high and low maxima in the same way as was seen in Fig. 5 at lower $T_1 E_0$. The ripples turn around a corner as they follow the contour lines in Fig. 4. Eventually, the remaining oscillations also disappear as we approach the DK2 region. This corresponds to moving between the C and D regions in Fig. 4. All the ripples disappear in region D because the DK2 expression shows no oscillations as a function of its parameters.

In Fig. 7 we see the probability P as a function of V_0/E_0 . Three different values of T_1 have been chosen to illustrate the different behavior for $T_1 < T_2$ and $T_1 > T_2$. For large V_0/E_0 the oscillations reach a fixed amplitude and period in each case. However, for smaller V_0/E_0 we see different qualitative behavior. There is an enhancement of probability in Fig. 7(a) where $T_1 > T_2$. In Fig. 7(b) we have $T_1 = T_2$ and the DK1 solution (13) applies showing an initial secant behavior followed by oscillations with a constant amplitude when $V_0 > E_0$. In Fig. 7(c) $T_1 < T_2$, and we see an alternating suppression and enhancement of the oscillations because of the different

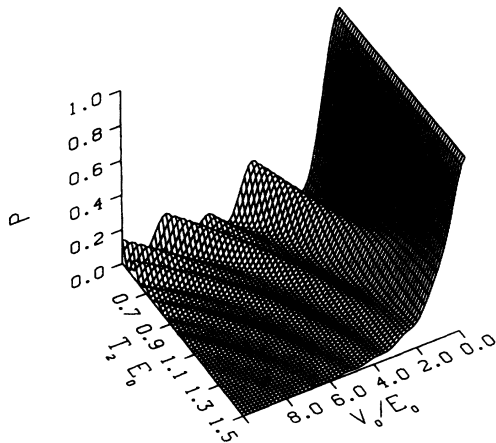


FIG. 6. This surface plot shows the value of the probability P over a portion of Fig. 4. The region selected is marked with a rectangle on Fig. 4 and shows nontrivial oscillations that disappear as the DK2 region is approached.

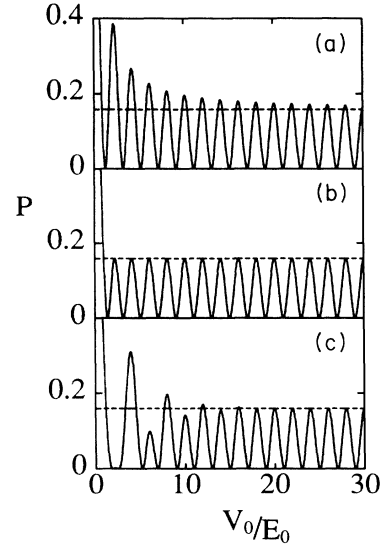


FIG. 7. This figure shows P as a function of the pulse strength V_0/E_0 . Exhibited are three different choices of parameters, and therefore three different types of envelopes for the oscillations. The time scales are $T_2 E_0 = 0.5$ and (a) $T_1 E_0 = 0.9$; (b) $T_1 E_0 = 0.5$ (the DK1 case); (c) $T_1 E_0 = 0.1$. The dashed horizontal line marks the limiting amplitude in the DK1 model.

places in Fig. 4 where the oscillations die out. We shall try and explain these features in Sec. III.

We can gain further understanding of the two-time-scale model by using the area theorem [4,12], which becomes applicable if the coupling totally dominates all other effects. The theorem may be obtained in the following way. First, we use the equation of motion Eq. (3) to form the second-order differential equation for C_1 only:

$$\frac{d^2 C_1}{dt^2} - \frac{\dot{V}}{V} \frac{dC_1}{dt} + \left[V^2 + \alpha^2 - i\dot{\alpha} + i\alpha \frac{\dot{V}}{V} \right] C_1 = 0. \quad (22)$$

Then if we let $\alpha, \dot{\alpha} \rightarrow 0$ and use our initial conditions, we may obtain the solution to this equation (omitting an inessential phase factor) as

$$C_1(t) = \cos \theta(t). \quad (23)$$

The function $\theta(t)$ is half the pulse ‘‘area’’ and is given by the integral

$$\theta(t) = \int_{-\infty}^t V(t') dt'. \quad (24)$$

In the case of the two-time-scale model we find that as $t \rightarrow \infty$,

$$\theta \rightarrow V_0 \int_{-\infty}^{\infty} \text{sech}^2(t'/T_2) dt' = \pi V_0 T_2, \quad (25)$$

which leads to the probability of finding the system in the original level 1,

$$P = \cos^2 \pi V_0 T_2. \quad (26)$$

Equation (26) shows oscillations as a function of V_0 and

T_2 similar to those seen in Fig. 7. However, the amplitude of the oscillations predicted by the area theorem is always unity, and so does not, in general, match the behavior of the two-time-scale model. In the case of the DK1 model, when $E_0/V_0 \rightarrow 0$ in the exact result (13), we find that

$$P \rightarrow \left[\frac{\cos \pi T V_0}{\cosh \pi T E_0} \right]^2. \quad (27)$$

So we can only obtain the area theorem prediction [Eq. (26) with $T_2 \rightarrow T$] if we have $\pi T E_0 \ll 1$. Interestingly, this condition is precisely the reverse of Eq. (15), the constraint on adiabaticity in the coupling.

The region where the area theorem is applicable is limited to small $T_2 E_0$ and large V_0/E_0 in the parameter space. However, this is because it gives the wrong amplitude for the oscillations. In general we find that the area theorem gives the positions of the oscillations very well if $V_0/E_0 \gg 1$. This can be seen in Fig. 8 where the dotted curves show the positions of the zeros of final probability as predicted by Eq. (26). These are curves for which $2V_0 T_2$ is an odd integer (though for clarity some of the curves have been omitted). The fit to the troughs in probability, indicated by the solid contour lines for $P=0.05$, is very good. We note that the DK1 expression is no longer useful at such a high value of $T_1 E_0$. For $V_0/E_0 > 1$ the amplitude of the oscillations in the DK1 model is $\text{sech}^2 \pi T_2 E_0$ [from Eq. (21)], and does not depend on V_0/E_0 . The vertical line in the figure shows where this amplitude lies at the level of the contour, $P=0.05$. If the DK1 expression were applicable, the solid contours would not pass to the right of the line as the oscillations would have insufficient amplitude in that region.

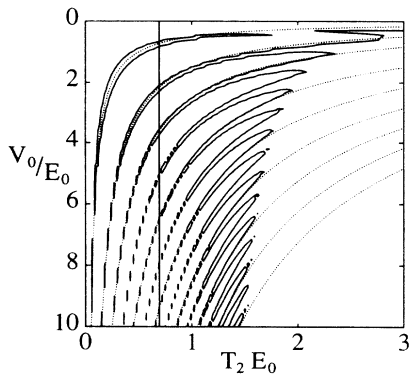


FIG. 8. This contour plot shows the single contour where $P=0.05$ for the parameter $T_1 E_0=10.0$. The comblike structure occurs because of oscillations in the probability as a function of the other parameters. The dotted lines are simple hyperbolas and have been determined from the area theorem. They show a good fit to the valleys in the probability surface. The vertical line would indicate the rightmost limit of the contours for $V_0/E_0 > 1$ if the DK1 model were applicable. In fact, it is not applicable because of the high value of $T_1 E_0$.

III. ADIABATICITY AND THE DYKHNE-DAVIS-PECHUKAS TREATMENT

When we look at the behavior of our model systems in the adiabatic limit, it is useful to consider the instantaneous eigenstates of the Hamiltonian Eq. (1). These states form the adiabatic basis. To transfer to that basis, we consider the unitary transformation $U(t)$ that will instantaneously diagonalize the Hamiltonian $H(t)$ so that

$$U(t)H(t)U^T(t) = \begin{bmatrix} -\mathcal{E} & 0 \\ 0 & \mathcal{E} \end{bmatrix}, \quad (28)$$

where \mathcal{E} is the quasienergy defined by

$$\mathcal{E}(t) = (\alpha^2 + V^2)^{1/2}. \quad (29)$$

The energy levels in the new basis will not cross, unless it happens that $\alpha(t)=V(t)=0$. However, we will be interested in crossings in the complex time plane. The unitary transformation required to carry out the diagonalization is

$$U = \begin{bmatrix} \cos \theta/2 & -\sin \theta/2 \\ \sin \theta/2 & \cos \theta/2 \end{bmatrix}, \quad (30)$$

with

$$\tan \theta = -V(t)/\alpha(t). \quad (31)$$

The new basis states Φ are given by

$$\Phi(t) = U(t)\Psi(t), \quad (32)$$

and they will obey a Schrödinger-like equation of motion

$$i \frac{d\Phi}{dt} = \begin{bmatrix} -\mathcal{E} & -i\gamma \\ i\gamma & \mathcal{E} \end{bmatrix} \Phi(t). \quad (33)$$

The time-dependent parameter γ is the nonadiabatic coupling,

$$\gamma = \frac{1}{2} \frac{d\theta}{dt} = \frac{1}{2} \frac{V\dot{\alpha} - \dot{V}\alpha}{\alpha^2 + V^2}. \quad (34)$$

If the nonadiabatic coupling is very small, the new basis will be nearly diagonal and the two states are almost uncoupled. If they were uncoupled it would be easy to solve the equations for the time dependence. Berry has extended this idea by considering successive transformations through a series of superadiabatic basis until the coupling does become small [13]. However, in general such a sequence is not expected to converge unless we are at the adiabatic limit, in which case the coupling γ can already be neglected in Eq. (33).

As long ago as the 1960s Dykhne had developed a non-perturbative method for evaluating transition probabilities in the adiabatic limit [14]. Dykhne's method employs the analytic continuation of the quasienergies into the complex time plane. He has shown that the adiabatic transition probability depends only on an integral of the quasienergy to a zero near to the origin on the complex plane. His result may be expressed as

$$P = \exp \left[-4 \operatorname{Im} \int_0^{t_c} \mathcal{E}(z) dz \right], \quad (35)$$

where t_c is the position of the zero, which must be in the upper half-plane. This zero is typically at a square-root branch point in the adiabatic energy surface and may be regarded as a complex crossing point. The probability P in Eq. (35) is actually defined to be the transition probability in the *adiabatic* basis, unlike the definition of P in Eq. (5). However, this makes no difference with most of the models considered in this paper because the adiabatic and diabatic states are the same when $t \rightarrow \pm \infty$. The exception is the DK2 model which has both a finite energy in the Hamiltonian and a finite coupling V_0 as $t \rightarrow \pm \infty$. We note that the probability P does not depend on the coupling $\gamma(t)$, a fact which is connected to being in the adiabatic limit.

Dykhne's work was later treated more rigorously by Davis and Pechukas who also suggested the idea of including contributions from more than one of the zeros in the complex plane if they are the same distance from the real axis [15]. Davis and Pechukas never gave any precise details of how to include additional zeros. However, we have suggested that the extension of Dykhne's formula could take the form [2,3]

$$P = \left| \sum_n \exp(i\Delta^{(n)}) \right|^2, \quad (36)$$

where $\Delta^{(n)}$ is the integral of the quasienergy from the origin to the n th zero, which is denoted as $t^{(n)}$,

$$\Delta^{(n)} = 2 \int_0^{t^{(n)}} \mathcal{E}(z) dz. \quad (37)$$

In general, we shall refer to the use of these nonperturbative methods as the DDP approach (after Dykhne-Davis-Pechukas). The coherent sum in Eq. (36) means that interferences can occur between contributions from the zeros. This feature can be interpreted as leading to the oscillations that may be found in the DK1 result Eq. (13). In that model there is a whole series of pairs of zeros in the complex plane. As we discussed in Ref. [3] these occur at the times

$$t^{(n)} = i(n + \frac{1}{2})\pi T \pm T \operatorname{arcosh}(V_0/E_0), \quad (38)$$

where n is an integer. Thus we see that for $V_0 > E_0$ the zeros are to be found symmetrically placed in pairs around the imaginary axis. As V_0 is reduced, the zeros move directly towards the imaginary axis where they meet if $V_0 = E_0$. We then have the exceptional point discussed in Ref. [3]. Further reductions in V_0 result in pairs of zeros moving away from each other along the imaginary axis. Eventually, as $V_0 \rightarrow 0$, we find one zero near the origin (in the upper half-plane), and a new pairing of zeros around each of the poles on the imaginary axis.

To evaluate probability (36) for the DK1 model, we keep only the first two zeros in the upper half-plane because for large V_0 these are at equal distances from the real axis. The integral of the quasienergy (37) is found to be [3]

$$\Delta^{(\pm)} = \pi T [iE_0 \pm (V_0^2 - E_0^2)^{1/2}] \quad (39)$$

for these zeros. This then leads to a probability

$$P = \{2 \exp(-\pi TE_0) \cosh[\pi T(E_0^2 - V_0^2)^{1/2}]\}^2, \quad (40)$$

which is remarkably close to the exact result Eq. (13). The difference is found in the factor $2 \exp(-\pi TE_0)$, which is the first term in the expansion of $\operatorname{sech}(\pi TE_0)$. The above result gives the correct behavior of the oscillations apart from an error in the amplitude. The oscillations themselves are seen to arise from the different signs of the real parts of the integrations to the zeros.

The Landau-Zener behavior discussed in Eq. (14) is found when there is a zero very close to the origin. The behavior of this zero dominates and it reproduces the Landau-Zener result (9); the Landau-Zener model itself has only a single zero in the upper half-plane.

We now turn to the DK2 model, where the quasienergy is

$$\mathcal{E} = [V_0^2 + E_0^2 \tanh^2(t/T_1)]^{1/2} \quad (41)$$

and the complex crossing times are found at

$$t^{(n)} = iT_1 [n\pi \pm \arctan(V_0/E_0)]. \quad (42)$$

We see that, unlike the DK1 model, these zeros are restricted to the imaginary axis for all values of the parameters. For low V_0 they lie in pairs between the poles in the quasienergy and as V_0 increases, they move towards the poles.

To carry out the DDP treatment, we consider only the single zero that lies between the origin and the first pole on the upper half-plane. In this case we find that the integral of the quasienergy $\Delta^{(0)}$ is a purely imaginary quantity and in Appendix B we show that

$$\Delta^{(0)} = i\pi T_1 [(E_0^2 + V_0^2)^{1/2} - E_0]. \quad (43)$$

The result for the DDP probability is then found from Eq. (36),

$$P = \exp\{-2\pi T_1 [(E_0^2 + V_0^2)^{1/2} - E_0]\}. \quad (44)$$

As in the DK1 case, we find that this is very close to the exact result. If we expand the two hyperbolic functions in Eq. (19), we obtain Eq. (44) by retaining only the first terms. The DDP result, like the exact result, shows no oscillations because the complex crossing point yields a purely imaginary quasienergy integral. As in the DK1 case, the Landau-Zener result is recovered if $V_0/E_0 \rightarrow 0$, which corresponds to the single zero moving close to the origin in the complex plane.

The quasienergy of the two-time-scale model is considerably more complicated than the DK1 and DK2 models. It has many poles on the imaginary axis of the complex plane, and it seems impossible to carry out the integration to the zeros by analytic methods, as we did with the DK1 and DK2 models. This means that we have to determine both the positions of the zeros and the integration of the quasienergy numerically. This may seem a little ironic; after all, why not simply carry out the numerical integration of Eqs. (3)? However, we are interested in carrying out a nontrivial test of the DDP method as well

as determining the adiabatic behavior. It may also be noted that as the adiabatic limit is approached, it can become quite difficult to carry out the numerical integration directly, because of the limited precision of computers. However, in that case it may still be feasible to carry out the numerical procedures for the DDP method.

The arrangement of the poles and zeros depends considerably on the relative sizes of the time scales T_1 and T_2 , as well as the coupling parameter V_0/E_0 . If $T_1 > T_2$ we will have a pair of zeros before the first pole for low values of V_0/E_0 . As V_0/E_0 is increased, these zeros move away from the imaginary axis and along curved paths that eventually are parallel to the real axis in the fashion of the DK1 model. Figure 9 shows several examples of this behavior; the data were generated by numerically determining the zeros in the quasienergy. In general there are an infinite number of pairs such as this, and the limiting value of the imaginary part of the position of the zero tends towards $(n + \frac{1}{2})\pi T_2$, for integer n . However, not all the zeros move off the imaginary axis in this way. Some may remain on the axis, where they move from near one pole to near an adjacent pole as V_0 is increased.

If we now change our regime to $T_1 < T_2$, the zero nearest the origin is found to be trapped before the first pole and is constrained to lie on the imaginary axis. Further, if $T_1 \ll T_2$, there are many zeros near the origin that lie on the axis and the situation very much resembles

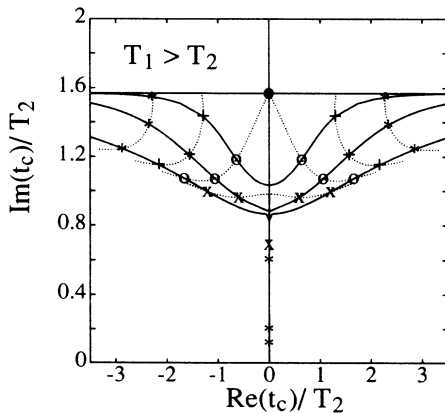


FIG. 9. The zero structure of quasienergy in the upper half of the complex time plane when $T_1 > T_2$. The zeros move in pairs along one of the solid lines towards the imaginary axis as V_0/E_0 decreases. The dotted lines show the tracks of the zeros if $\gamma = T_1/T_2$ is changed with V_0/E_0 fixed. If γ is reduced towards unity, the zeros approach the horizontal line for which $\text{Im}(t_c/T_2) = \pi/2$. The parameters for the three solid curves are $\gamma = 5.0, 2.0$, and 1.2 , from the lower to the upper curve. The markers on them are for selected values of V_0/E_0 , namely * for 5.0 , + for 3.0 , O for 1.0 , and X for 0.5 . We note that for the last case, when $\gamma = 1.2$ and $V_0/E_0 = 0.5$, both the zeros marked X lie on the imaginary axis, but only the lower one is shown. The three asterisks that lie on the imaginary axis correspond to $V_0/E_0 = 0.1$ and the three values of γ . The black dot at the crossing of the horizontal and vertical solid lines shows the position of the pole at $t_c/T_2 = i\pi/2$.

the DK2 model. So it is no surprise that this is the parameter range where we found in Sec. II that the DK2 model applied. However, if we go far enough up the imaginary axis, we will eventually find a pair of zeros of the DK1 type; that is, a pair that may leave the axis as V_0/E_0 is increased.

Figure 10 shows three examples of this. The two solid curves and the horizontal line show the tracks of pairs of zeros as V_0/E_0 is changed. For the lower curve, $T_1 = 0.42T_2$, and we see the behavior of the third and fourth zeros on the complex plane. These zeros lie above the first pole. The first and second zeros are trapped below and above the pole, respectively. On the upper curve, $T_1 = 0.88T_2$, and we again see the behavior of the third and fourth zeros, but this time they lie above two poles. The second zero is trapped between the poles, and the first zero lies in front of the poles. The horizontal line shows a somewhat exceptional track. If $T_2 = 2NT_1$, where N is an integer, we find that some of the zeros move along straight lines as in the DK1 case, but they can never reach the imaginary axis except in the limit $V_0/E_0 \rightarrow 0$.

The examples of Fig. 10 are cases where we have one zero near the origin and two other off-axis zeros nearby. This is not a situation we have met before in the Landau-Zener, DK1, or DK2 models. In carrying out the DDP integrations we have included contributions from all three zeros when they are present (i.e., for $T_1 < T_2$).

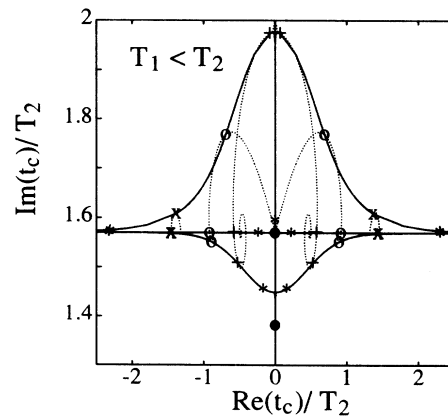


FIG. 10. The zero structure of quasienergy in the upper half of the complex time plane when $T_1 < T_2$. The zeros move in pairs along one of the solid lines towards the imaginary axis as V_0/E_0 decreases. The dotted spirals show the tracks of the zeros if $\gamma = T_1/T_2$ is changed with V_0/E_0 fixed. If γ is reduced towards zero, the tracks approach the horizontal line for which $\text{Im}(t_c/T_2) = \pi/2$. The parameters for the three solid curves are $\gamma = 0.42, 0.5$, and 0.88 , from bottom to top. The markers on them have the following associations with selected values of V_0/E_0 : * for 5.0 , X for 2.0 , O for 1.0 , and + for 0.5 . The symbol * is also used for $V_0/E_0 = 0.1$ near the imaginary axis. When $\gamma = 0.88$ the * lies on the axis. The upper black dot is the pole at $t_c/T_2 = i\pi/2$ and the lower dot is the pole at $t_c/T_1 = i\pi/2$ when $\gamma = 0.88$. For the other values of γ this lower pole does not appear on the figure.

Zeros that hide behind poles have not been included. From the symmetry properties of the quasienergy we can show that for the zero lying on the imaginary axis the Δ integral Eq. (37) must be imaginary; we will write it as $\Delta^{(0)} = i\Delta_i^0$. The integrals for the two off-axis, or DK1-type, zeros will take the form

$$\Delta^{(\pm)} = \pm\Delta_r + i\Delta_i. \tag{45}$$

If we use these expressions we find that the probability Eq. (36) becomes

$$P = [\exp(-\Delta_i^0) + 2\exp(-\Delta_r)\cos\Delta_r]^2. \tag{46}$$

For large V_0/E_0 we find that Δ_r changes rapidly, while Δ_i and Δ_i^0 change slowly. This means that we obtain a double-envelope function that oscillates between zero and $[\exp(-\Delta_i^0) + 2\exp(-\Delta_r)]^2$, and between zero and $[\exp(-\Delta_i^0) - 2\exp(-\Delta_r)]^2$ in the manner of the exact behavior seen in Figs. 5 and 7(c). For very large V_0/E_0 the two envelopes merge because Δ_i^0 becomes large. By evaluating the functions $\Delta^{(n)}$ numerically we can obtain quite a good match between Eq. (46) above and the exact result, provided that $P \ll 1$, and especially for large V_0/E_0 and large T_2E_0 . If $T_1 > T_2$ we simply omit the $\exp(-\Delta_i^0)$ term as the third zero is not present.

We have also been able to improve on the result by means of two modifications to Eq. (46) above. The first change is strongly suggested by the comparison of the exact and approximate DK1 results, namely Eqs. (13) and (40). We replace the factor $2\exp(-\Delta_r)$ by the hyperbolic secant function of which it is a limit: $\text{sech}(\Delta_r)$. The second change is to replace the first term in Eq. (46) by the factor

$$\sinh(\pi T_1 E_0) \text{cosech} [\pi T_1 (E_0^2 + V_0^2)^{1/2}],$$

suggested by the exact result for the DK2 problem in Eq. (19). Thus, on using this prescription, we obtain

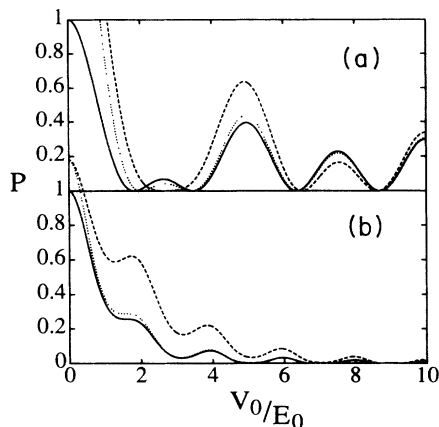


FIG. 11. This figure shows a comparison between the numerical result for the two-time-scale model (solid curve) and two types of DDP calculation. The dashed curve shows the DDP calculation given in Eq. (46), and the dotted curve the result from the modified DDP calculation of Eq. (47). The latter gives a somewhat better fit. The parameters are $T_1E_0 = 0.1$, and (a) $T_2E_0 = 0.4$; (b) $T_2E_0 = 1.0$.

$$P = \{ \sinh(\pi T_1 E_0) \text{cosech} [\pi T_1 (E_0^2 + V_0^2)^{1/2}] + \text{sech}(\Delta_r) \cos\Delta_r \}^2. \tag{47}$$

This gives a reasonable approximation to the exact behavior over quite a wide range of the parameters. For example, in Fig. 4, it turns out that there is a good fit for $V_0/E_0 > 3$, which becomes better as T_2E_0 increases. And in Fig. 5, the dotted line shows a close match between the numerical data and Eq. (47) with Δ_i and Δ_r calculated using the DK1 model. This demonstrates a good result for T_2E_0 smaller than unity, as long as V_0/E_0 is large and $T_1 \ll T_2$. For small P the double envelope structure is reproduced quite well.

In Fig. 11 we see that if we have a large value of V_0/E_0 , the dotted line obtained from Eq. (47) follows the exact result closely. This may be compared to the dashed

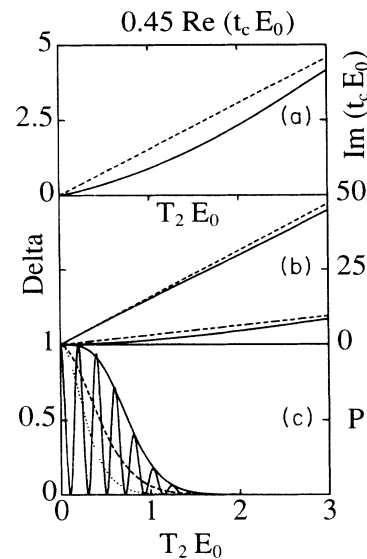


FIG. 12. This figure shows a comparison between final probabilities calculated from the two-time-scale model, the DK1 model, and the DDP calculation in a case where we consider two complex crossing points. The parameters are $V_0/E_0 = T_1E_0 = 5.0$. In (a) we show the track of the zero (or crossing point) in the first quadrant of the complex plane and as a function of T_2E_0 . The solid curve shows the exact result, obtained by numerical integration, and the dashed line shows the linear track predicted by the DK1 model where T_1 follows T_2 . In (b) we see the integrals Δ_r (upper pair) and Δ_i (lower pair). The values can be read from the right-hand-side scale, and again the numerical result is shown as the solid curve and the dashed line shows the analytic DK1 result. In (c) the oscillating curve is the numerical result for the probability and the remaining curves are approximations to the envelope of the oscillations. The DK1 envelope is shown as the dotted curve, the straightforward DDP envelope [Eq. (46) with Δ_r set to zero] is shown as the dashed curve, and the modified DDP envelope [Eq. (47) with Δ_r set to zero] is shown with a solid line. In the latter case, if the oscillations are included (Δ_r is used as computed) we find a near-perfect fit where the differences cannot be seen by the eye.

line in the same figure, which shows results obtained by using Eq. (46). In Fig. 11(b) we can see that by increasing $T_2 E_0$ the approach to the exact result is improved, and the staircase structure indicating a strong mixture of the DK1 and DK2 contributions is reproduced quite well. Usually, when Eq. (47) starts to be a worse approximation than Eq. (46), we are already well within the region where they both cease to be useful.

Figure 12 shows a case where the fit of Eq. (47) is so good that the difference can hardly be seen. Because $T_1 > T_2$ only the latter part of Eq. (47) is used, resulting in the single-envelope structure that resembles the DK1 model. This is because both the track of the zeros in the complex plane and the Δ integrals are close to the DK1 model, as may be seen in Figs. 12(a) and 12(b). However, both the DK1 probability and the calculation from Eq. (46) give poor results. To make a comparison, we have plotted only the envelopes of the results from these calculations (as the dotted and dashed curves). These may be compared to the envelope from Eq. (47) (shown solid), and to the exact numerical data.

As shown with the examples above, Eq. (47) has quite a wide applicability. This suggests that, for other models, it may be possible in the future to improve on the general formula of Eq. (36).

IV. CONCLUSION

We have examined probability transfer in the two-time-scale model over a wide range of parameters and have discovered several layers in the understanding of its behavior. At the simplest level, we can approximate the model by the exponential behavior of the Landau-Zener model, or, for different parameters, by oscillatory behavior characteristic of the area theorem or the Rosen-Zener model.

At the next level of understanding, we can approximate the model behavior by using the first and second Demkov-Kunike models. These apply to mutually exclusive areas of the parameter space, and contain within them the Landau-Zener model and the area theorem result. We have been able to show why the second Demkov-Kunike model is applicable through a simple intuitive argument, and further support for both cases comes from the DDP analysis in the complex plane.

At the innermost level of our understanding, we perceive that the Demkov-Kunike models are applicable because they provide a sequence of complex crossing points that approximate the real situation in the two-time-scale model. We have extended the idea in two ways. First, we have considered a DDP analysis with three complex crossing points and have found this to be successful in describing features of the model not covered by the Demkov-Kunike models. Second, we have discovered an extension of the DDP analysis which, at least in the two-time-scale model, provides an excellent account of the probability transfer. The extension suggests that the two-time-scale model can be regarded as a coherent superposition of both the Demkov-Kunike models over a large part of the parameter space.

ACKNOWLEDGMENT

We wish to thank Professor Stig Stenholm for many useful discussions and practical advice before and during the preparation of this article.

APPENDIX A: THE DEMKOV-KUNIKE SOLUTIONS

In this appendix we wish to show how Eqs. (13) and (19) are obtained by reproducing, in an abbreviated form, the analysis given by Demkov and Kunike in Ref. [9]. The first Demkov-Kunike (DK1) model is defined in its full form by

$$\begin{aligned} \alpha(t) &= a + b \tanh t / T, \\ V(t) &= c \operatorname{sech} t / T. \end{aligned} \tag{A1}$$

When α and V are inserted into Eqs. (1)–(3) [or Eq. (22)] we obtain

$$\begin{aligned} \frac{d^2 C_1}{dt^2} + \frac{1}{T} \tanh \frac{t}{T} \frac{dC_1}{dt} + \left[c^2 \operatorname{sech}^2 \frac{t}{T} + \left(a + b \tanh \frac{t}{T} \right)^2 \right. \\ \left. + i \frac{1}{T} \left[a \tanh \frac{t}{T} + b \right] \right] C_1 = 0. \end{aligned} \tag{A2}$$

If we substitute

$$\tanh t / T = 2z - 1 \tag{A3}$$

into Eq. (A2) we obtain the Gauss equation,

$$\begin{aligned} \frac{d^2 C_1}{dz^2} + \frac{1}{2} \left[\frac{1}{z} + \frac{1}{z-1} \right] \frac{dC_1}{dz} + \frac{T^2}{4} \left[\frac{(a-b)^2 - i(a-b)/T}{z^2} + \frac{(a+b)^2 + i(a+b)/T}{(z-1)^2} \right. \\ \left. + 2(a^2 - b^2 + 2c^2 + ib/T) \left[\frac{1}{z} - \frac{1}{z-1} \right] \right] C_1 = 0. \end{aligned} \tag{A4}$$

If one sets for C_1 the ansatz

$$C_1 = z^{-iT(a-b)/2} (z-1)^{iT(a+b)/2} u(z), \tag{A5}$$

then $u(z)$ has to satisfy the hypergeometric equation. The initial conditions are given at $t \rightarrow -\infty$, that is at $z = 0$, so the general solution is constructed in the vicinity of that point:

$$u(z) = AF(iT[b + (b^2 - c^2)^{1/2}], iT[b - (b^2 - c^2)^{1/2}]; \frac{1}{2} - iT(a - b); z) \\ + Bz^{1/2 + iT(a - b)} F(\frac{1}{2} + iT[a + (b^2 - c^2)^{1/2}], \frac{1}{2} + iT[a - (b^2 - c^2)^{1/2}]; \frac{3}{2} + iT(a - b); z), \quad (\text{A6})$$

where A and B are arbitrary constants, and $F(k, l; m; z)$ is the hypergeometric function. Inserting $u(z)$ into Eq. (A5) with the initial conditions Eq. (4), we will find

$$C_1(z) = \pm z^{-iT(a - b)/2} (1 - z)^{iT(a + b)/2} F(iT[b + (b^2 - c^2)^{1/2}], iT[b - (b^2 - c^2)^{1/2}]; \frac{1}{2} - iT(a - b); z). \quad (\text{A7})$$

With the mutual relations between the solutions of the hypergeometric equation in the vicinity of the points $z = 0$ and $z = 1$ we obtain

$$C_1(z) = \pm \{ z^{-iT(a - b)/2} (1 - z)^{iT(a + b)/2} G_1 F(iT[b + (b^2 - c^2)^{1/2}], iT[b - (b^2 - c^2)^{1/2}]; \frac{1}{2} + iT(a + b); 1 - z) \\ + z^{-iT(a - b)/2} (1 - z)^{1/2 - iT(a + b)/2} G_2 \\ \times F(\frac{1}{2} - iT[a - (b^2 - c^2)^{1/2}], \frac{1}{2} - iT[a + (b^2 - c^2)^{1/2}]; \frac{3}{2} + iT(a + b); 1 - z) \}. \quad (\text{A8})$$

Here,

$$G_1 = \frac{\Gamma(\frac{1}{2} - iT(a - b)) \Gamma(\frac{1}{2} - iT(a + b))}{\Gamma(\frac{1}{2} - iT[a + (b^2 - c^2)^{1/2}]) \Gamma(\frac{1}{2} - iT[a - (b^2 - c^2)^{1/2}])}, \quad (\text{A9})$$

$$G_2 = \frac{\Gamma(\frac{1}{2} - iT(a - b)) \Gamma(\frac{1}{2} - iT(a + b))}{\Gamma(iT[b + (b^2 - c^2)^{1/2}]) \Gamma(iT[b - (b^2 - c^2)^{1/2}])}, \quad (\text{A10})$$

where $\Gamma(k)$ is the gamma function.

Hence, from Eq. (A8), and taking into account the fact that (i) if $a > b$ there is no crossing of terms in the absence of the interaction, and (ii) if $a < b$ the crossing exists, we obtain for the final population of level 1

$$P = \begin{cases} \frac{\sinh \pi T [b + (b^2 - c^2)^{1/2}] \sinh \pi T [b - (b^2 - c^2)^{1/2}]}{\cosh \pi T (a + b) \cosh \pi T (a - b)}, & a > b \\ \frac{\cosh \pi T [a + (b^2 - c^2)^{1/2}] \cosh \pi T [a - (b^2 - c^2)^{1/2}]}{\cosh \pi T (a + b) \cosh \pi T (a - b)}, & a < b. \end{cases} \quad (\text{A11})$$

In the second Demkov-Kunike model (DK2 model) we have

$$\alpha(t) = a + b \tanh t / T, \quad (\text{A12}) \\ V(t) = c,$$

where c is a constant. The calculation of the level populations is carried out in the same way as previously. This time by substituting Eq. (A12) into Eqs. (1)–(3) or (22) we will find equations for C_1 and C_2 in the form

$$\frac{d^2 C_1}{dt^2} + [(a + b \tanh t / T)^2 \\ + c^2 + ib(1 - \tanh^2 t / T)] C_1 = 0, \quad (\text{A13})$$

$$C_2 = \frac{i}{c} \frac{dC_1}{dt} - \frac{(a + b \tanh t / T)}{c} C_1. \quad (\text{A14})$$

In Eq. (A13) we may now make the substitution Eq. (A3) that we previously used in Eq. (A2). This time we obtain a Gauss equation with the solution

$$C_1 = z^{iE_a T/2} (z - 1)^{iE_e T/2} v(z), \quad (\text{A15})$$

where instead of the parameters a, b, c we have $E_a = |[(a - b)^2 + c^2]^{1/2}|$, $E_e = |[(a + b)^2 + c^2]^{1/2}|$, and b . The function $v(z)$ is a solution of the hypergeometric equation.

In this case, the initial condition have to be set in the adiabatic basis, and this involves a mixture of C_1 and C_2 . We will then obtain

$$C_1 = Bz^{-iE_a T/2} (z - 1)^{iE_e T/2} F\left[1 + \frac{iT}{2}(-E_a + E_e + 2b), \frac{iT}{2}(-E_a + E_e - 2b); 1 - iT E_a; z\right], \quad (\text{A16})$$

where

$$B = \sqrt{(E_a + E_e - 2b)(E_e - E_a + 2b) / 8bE_a}$$

is a constant.

By using Eq. (A14) we obtain the function C_2 . Then on using the initial conditions given in the adiabatic basis we finally obtain, from both C_1 and C_2 ,

$$P = \frac{\sinh[\pi T(E_e - E_a + 2b)/2] \sinh[\pi T(E_a - E_e + 2b)/2]}{\sinh \pi t E_a \sinh \pi T E_e} . \quad (\text{A17})$$

This is the DK2 solution, given in the adiabatic basis. We note that in this case the adiabatic states do not correspond to the diabatic states when $t \rightarrow \pm \infty$. This is quite different from the DK1 model.

APPENDIX B: THE INTEGRAL $\Delta^{(0)}$ FOR THE DK2 MODEL

The integral is to be taken from the origin to the first complex crossing point

$$t^{(0)} = iT_1 \arctan(V_0/E_0) \quad (\text{B1})$$

as given by Eq. (42). By changing the integration variable to the imaginary time $x = -it/T_1$ we find that Eq. (37) takes the form

$$\Delta^{(0)} = 2iT_1 \int_0^{x^{(0)}} (V_0^2 - E_0^2 \tan^2 x)^{1/2} dx , \quad (\text{B2})$$

with

$$\tan x^{(0)} = V_0/E_0 . \quad (\text{B3})$$

If we now set $C^2 = 1 + (E_0/V_0)^2$ and $D^2 = 1 - C^2$ we find that

$$\Delta^{(0)} = 2iT_1 V_0 \int_0^{x^{(0)}} \sec x (1 - C^2 \sin^2 x)^{1/2} dx , \quad (\text{B4})$$

and thus (see, e.g., Ref. [16]),

$$\Delta^{(0)} = 2iT_1 V_0 \left[\frac{D}{2} \ln \frac{(1 - C^2 \sin^2 x)^{1/2} + D \sin x}{(1 - C^2 \sin^2 x)^{1/2} - D \sin x} + C \arcsin(C \sin x) \right] \Bigg|_{x=0}^{x=x^{(0)}} . \quad (\text{B5})$$

Using the fact that $\sin x^{(0)} = V_0/(V_0^2 + E_0^2)^{1/2}$ we will now obtain the result, Eq. (43),

$$\Delta^{(0)} = i\pi T_1 [(E_0^2 + V_0^2)^{1/2} - E_0] . \quad (\text{B6})$$

-
- [1] See, for example, *Geometric Phases in Physics*, edited by A. Shapere and F. Wilczek (World Scientific, Singapore, 1989).
- [2] B. M. Garraway, K. -A. Suominen, and S. Stenholm, *Light Induced Kinetic Effects on Atoms, Ions, and Molecules*, edited by L. Moi, S. Gozzini, C. Gabbianini, E. Arimondo, and F. Strumia (Ets Editrice, Pisa, 1991), p. 129.
- [3] K. -A. Suominen, B. M. Garraway, and S. Stenholm, *Opt. Commun.* **82**, 260 (1991).
- [4] L. Allen and J. H. Eberly, *Optical Resonance and Two-Level Atoms* (Wiley, New York, 1975).
- [5] B. Shore, *The Theory of Coherent Atomic Excitation* (Wiley, New York, 1990), Vol. 1.
- [6] J. R. Rubbmark, M. M. Cash, M. G. Littman, and D. Kleppner, *Phys. Rev. A* **23**, 3107 (1981).
- [7] W. van de Water, S. Yoakum, T. van Leeuwen, B. E. Sauer, L. Moorman, E. J. Galvez, D. R. Mariani, and P. M. Koch, *Phys. Rev. A* **42**, 572 (1990).
- [8] L. D. Landau, *Phys. Z. Sowjetunion* **2**, 46 (1932); C. Zener, *Proc. R. Soc. London Ser. A* **137**, 696 (1932).
- [9] Yu. N. Demkov and M. Kunike, *Vestn. Leningr. Univ. Fis. Khim.* **16**, 39 (1969).
- [10] F. T. Hioe, *Phys. Rev. A* **30**, 2100 (1984); F. T. Hioe and C. E. Carroll, *J. Opt. Soc. Am. B* **2**, 497 (1985).
- [11] N. Rosen and C. Zener, *Phys. Rev.* **40**, 502 (1932).
- [12] S. L. McCall and E. L. Hahn, *Phys. Rev.* **183**, 457 (1969).
- [13] M. V. Berry, *Proc. R. Soc. London Ser. A* **429**, 61 (1990).
- [14] A. M. Dykhne, *Zh. Eksp. Teor. Fiz.* **38**, 570 (1960) [*Sov. Phys.—JETP* **11**, 411 (1960)]; **41**, 1324 (1961) [**14**, 941 (1962)].
- [15] J. P. Davis and P. Pechukas, *J. Chem. Phys.* **64**, 3129 (1976).
- [16] I. S. Gradshteyn and I. M. Ryzhik, *Table of Integrals, Series, and Products* (Academic, New York, 1980), p. 160.

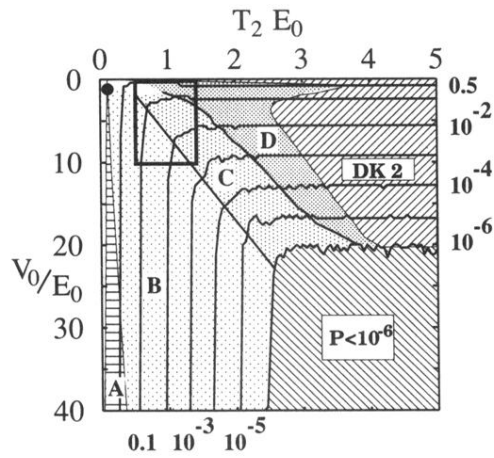


FIG. 4. This diagram shows how the final probability may be characterized over a region of the parameter space with $T_1 E_0 = 0.1$. The axes for V_0/E_0 and $T_2 E_0$ are to the left-hand side and above, respectively. The numbers displayed on the right-hand side and below are values belonging to the contour lines. The contours themselves are found by taking peak values when oscillatory behavior is present (in regions A, B, C, and D). The computational precision prevents any designation to the region in the bottom right-hand-side corner. The rectangle near the top left-hand-side corner shows the area covered by Fig. 6. The black dot marks the exceptional point discussed in the text. Regions A and B exhibit behavior related to the DK1 model. Regions C and D show complex oscillatory structures that do not belong to any simple model, but that may be partially described using the methods of Sec. III.